IEEE Access
Multidisciplinary | Rapid Review | Open Access Journal

Received December 2, 2020, accepted December 30, 2020, date of publication January 18, 2021, date of current version January 29, 2021.

Digital Object Identifier 10.1109/ACCESS.2021.3052484

0.7-1.0-GHz Switchable Dual-/Single-Band Tunable Bandpass Filter Using a Switchable J-Inverter

YOUNG-HO CHO[1], (Member, IEEE), CHEOLSOO PARK[2], (Member, IEEE), AND SANG-WON YUN[3], (Life Member, IEEE)

[1]Department of Electrical and Communication Engineering, Daelim University, Kyoung 13916, South Korea
[2]Department of Computer Engineering, Kwangwoon University, Seoul 01897, South Korea
[3]Department of Electronics, Sogang University, Seoul 04107, South Korea

Corresponding authors: Cheolsoo Park (parkcheolsoo@kw.ac.kr) and Sang-Won Yun (swyun@sogang.ac.kr)

This work was supported by the National Research Foundation of Korea (NRF) under grant funded by the Korean Government (MSIT) under Grant NRF-2017R1A5A1015596.

ABSTRACT Cognitive radios require tunable band-switchable bandpass filters to respond to the dynamically changing operating frequencies in cognitive systems. This study presents a novel switchable dual-/single-band tunable bandpass filter using a single switchable J-inverter. The proposed filter configuration can be easily converted from a two-pole dual-passband mode to a four-pole single-passband mode using the single J-inverter with switches. This is achieved through a novel dual-band bandpass filter configuration using hybrid resonators that consist of two parallel resonators and one J-inverter. In addition, two bandwidths and two center frequencies of the dual-passband mode are designed, and a high stopband attenuation level is achieved due to a transmission zero between the two passbands. The proposed filter is built on a Duroid substrate with a dielectric constant of 3.48 and a thickness of 30 mil. The tuning of the center frequency and the passband number change are carried out using silicon varactors and PIN diodes. In the four-pole single-passband mode, a center frequency tuning of 0.75–1.08 GHz is achieved with 1-dB bandwidths of 105–158 MHz. The two-pole dual-band bandpass filter mode has a center frequency tuning of 0.69–0.9 GHz (low-band) and 0.85–1.07 GHz (high-band). It has potential for application in wideband cognitive radios.

INDEX TERMS Tunable filter, switchable-band, dual-band, single-band, bandpass filter.

I. INTRODUCTION

Cognitive radios have the potential to improve spectrum efficiency using dynamic frequency-agile front-end receivers [1]. As the number of operating frequencies in cognitive systems changes dynamically, tunable band-switchable bandpass filters are required to respond to the desired frequencies, as shown in Fig. 1. Tunable band-switchable filters are microwave components with passband number change [2], [3] and center frequency tunability [4], [5], simultaneously. When a cognitive radio is operated at a single frequency or two frequencies, the single-band or dual-band bandpass filter is selected, respectively, and the center frequencies are tuned.

Recently, several tunable band-switchable bandpass filters have been demonstrated. The band-switchable filters with center frequency tunability have been developed using varactor-loaded resonators [6]. As one passband is removed based on the impedance mismatching technique, the resonant poles still remain on the out-band, and thus a low stopband attenuation level is shown. Additionally, a center-frequency-tuned band-switchable filter was realized based on a membrane-shorting method [7], where the number of passbands is mechanically tuned. Also, the tunable band-switchable filter was designed based on the transmission pole relocation method. However, the dual-passband

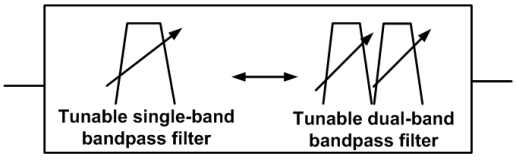

FIGURE 1. Concept of a tunable bandpass filter with switchable dual-/single-passband modes.

The associate editor coordinating the review of this manuscript and approving it for publication was Abhishek K. Jha.

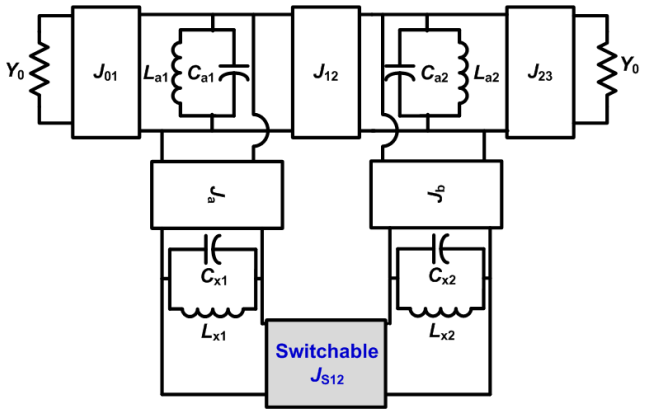

FIGURE 2. Proposed bandpass filter circuit with switchable four-pole single- / two-pole dual-passband modes using a single switchable *J*-inverter.

mode stopband attenuation characteristic is poor [8]. PIN diodes have typically been used to obtain a switchable-band bandpass filter with a high attenuation characteristic [2], [3], but the number of the PIN diodes should be reduced.

In this article, a novel tunable bandpass filter with switchable four-pole single-band/two-pole dual-band responses is proposed based on a single switchable J-inverter (J_{S12}) with PIN diode switches, as shown in Fig. 2. The proposed method is considered to have five main benefits in comparison with the conventional design method.

First, the proposed filter configuration is easily converted from a two-pole dual-passband mode to a four-pole single-passband mode using just the single J-inverter. This is accomplished based on a filter configuration using hybrid resonators with both series and parallel resonances. These filters have two passbands owing to the insertion of a transmission zero in the wide passband [9]. Fig. 3(a) and (b) show the conventional hybrid resonator-based dual-band bandpass filter structures [9], [10]. The hybrid resonator in Fig. 3(a) was designed using both the series and parallel resonators [9]. In order to transform the dual-passband characteristic to a single-passband, the transmission zero between the two passbands should be eliminated. However, it is difficult to eliminate it due to the existence of the series resonator. In the filter design in Fig. 3(b), the hybrid resonator was realized with two series resonators and one J-inverter, which had difficulty obtaining the switchable-band response due to the series resonator [10]. Moreover, two bandwidths cannot be controlled independently. In the proposed dual-band bandpass filter configuration in Fig. 3(c), the hybrid resonator is accomplished using two parallel resonators and one J-inverter. As shown in Fig. 2, a four-pole single-passband mode is obtained by applying just one switchable J-inverter between two parallel resonators (C_{x1}/L_{x1} and C_{x2}/L_{x2}). When the switch included in J_{S12} of the filter shown in Fig. 2 is in the off-state, the two-pole dual-passband response is achieved as shown in Fig. 3(c). Conversely, when the switch is in the on-state, the dual-band bandpass filter is transformed into a four-pole single bandpass filter with cross coupling. J_{12} becomes the

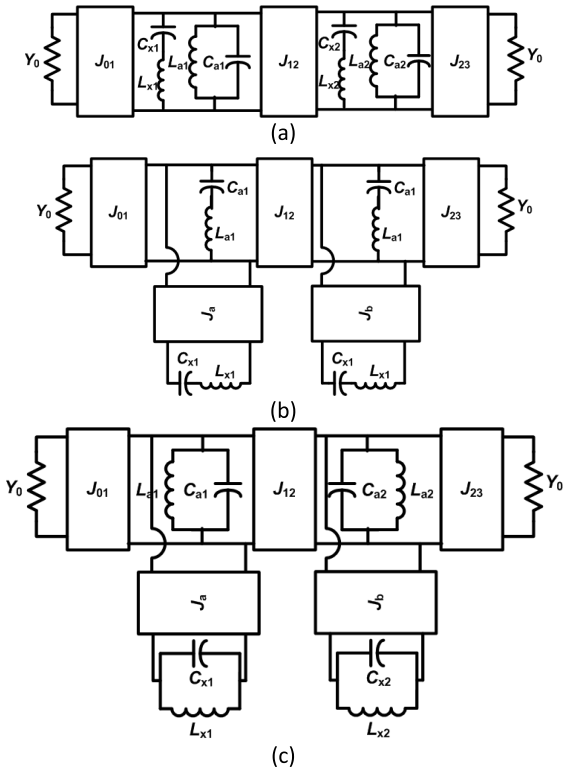

FIGURE 3. Conventional two-pole hybrid resonator-based dual-band bandpass filter prototypes presented in (a) [9], and (b) [10], and (c) the proposed two-pole dual-band bandpass filter prototype.

cross coupling, and J_a, J_{S12}, and J_b operate as J-inverters between the resonators.

Second, two bandwidths and two center frequencies for the dual-passband mode are designed based on the dual-band filter configuration in Fig. 3(c). Two center frequencies of the conventional switchable-band filters presented in [6]-[8] are located at a distance from each other to obtain a high attenuation level between the two passbands. However, as the proposed filter has a transmission zero between the passbands, the center frequencies are easily determined with the high stopband attenuation level. In addition, we present the design method to control two bandwidths based on the filter structure in Fig. 3(c).

Third, the two-pole dual-passband mode is transformed into a four-pole single-passband mode thereby increasing the number of poles for the single-passband. In the conventional design suggested in [6], [7], the two-pole dual-passband mode is changed to a two-pole single-passband mode, as two poles among the four poles for the dual-passband mode are eliminated to obtain a single-passband response. Alternately, in the proposed design, the four-pole wide single-passband mode is achieved using entire poles for the dual-passband mode.

Moreover, the proposed filter achieves a high stopband attenuation level between the two passbands in the dual-passband mode compared with the existing design methods in [6]–[8] due to the transmission zero between them. The attenuation level for the single-passband mode is also enhanced compared to the filters in [6]–[8], as one of the two

passbands is removed based on the proposed filter configuration in Fig. 2.

Finally, as the PIN diode switch is included in the J-inverter instead of the filter resonators, the quality factor (Q) and electrical length of the resonator in the proposed filter configuration are hardly affected by the switch's parasitic elements.

II. FILTER DESIGN

A. PROPOSED FILTER PROTOTYPE

The filter configuration in Fig. 3(c) is achieved by implementing J-inverters in the circuit in Fig. 4 [10]. The series resonator is operated as a capacitor on lower frequencies and an inductor on higher frequencies than its series resonance, and the parallel resonator functions in opposition to the series resonator. Therefore, when the resonant frequencies for the series and parallel resonators are equal, two resonances are obtained at lower and higher frequencies than the resonant frequency of the series and parallel resonators (see Fig. 4) [9]. Therefore, the proposed filter in Fig. 3(c) has two passbands.

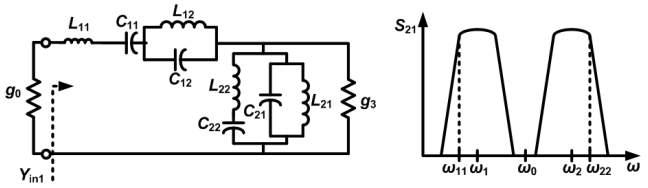

FIGURE 4. Two-pole dual-band bandpass filter prototype using series and parallel resonators.

As shown in Fig. 2, when a J-inverter (J_{S12}) is added in the filter circuit in Fig. 3(c) and the switch is in on-state, the filter can be operated as a four-pole single-band bandpass filter performance with cross coupling. The four poles in the passband are realized using the four resonators (L_{a1}/C_{a1}, C_{x1}/L_{x1}, L_{x2}/C_{x2}, and C_{a2}/L_{a2}). J_{01} and J_{23} are the input/output impedance/admittance inverters, and J_a, J_{S12}, and J_b are operated as J-inverters between the resonators. In addition, J_{12} functions as the cross coupling. On the other hand, when the J_{12} is in off-state, the filter structure with the dual-passband mode in Fig. 3(c) is obtained.

Therefore, based on the filter prototype in Fig. 2, the tunable bandpass filter with the switchable four-pole single- / two-pole dual-passband modes is accomplished using a single switchable J-inverter.

B. EXTRACTION OF DUAL-BAND BANDPASS FILTER PARAMETERS

The dual-band bandpass filter parameters are extracted according to the procedure in [10]. However, the filter suggested in [10] was designed using series-resonators, and it is difficult to control the bandwidths and obtain a switchable-band response. This article suggests the design procedure using the parallel resonators for the switchable-band performance, the good attenuation characteristic, and the bandwidth control.

A lowpass filter prototype is transformed into a dual-band bandpass filter using (1) and (2).

$$\Omega = \frac{1}{\alpha}\left(\frac{\omega'}{\beta} - \frac{\chi}{\omega'}\right), \tag{1}$$

$$\omega' = \frac{\beta}{\gamma}\left(\frac{\omega}{\beta} - \frac{\chi}{\omega}\right). \tag{2}$$

When $\Omega = 0$, two center frequencies ($\omega = \omega_1$ and ω_2) are obtained, as shown in Fig. 4 [10]. ω_1 and ω_2 are the lower and higher center frequencies, respectively. When $\Omega = 0$, ω' is extracted from (1) as

$$\omega' = \pm\sqrt{\beta\chi}. \tag{3}$$

If (3) is substituted into (2), γ and β are calculated as

$$\gamma = \frac{\omega_2 - \omega_1}{\sqrt{\omega_1\omega_2}}, \tag{4}$$

$$\beta = \frac{\omega_1\omega_2}{\chi}. \tag{5}$$

To control the bandwidths, the following procedure is added to the method introduced in [10]. When $\Omega = 1$, the cutoff frequencies ($\omega = \omega_{11}$ and ω_{22}) are obtained (see Fig. 4). When $\Omega = 1$, ω' is calculated from (1) as

$$\omega' = \frac{\alpha\beta + \sqrt{(\alpha\beta)^2 + 4\chi\beta}}{2}, \tag{6}$$

$$omega' = \frac{-\alpha\beta - \sqrt{(\alpha\beta)^2 + 4\chi\beta}}{2}. \tag{7}$$

When (6) and (7) are inserted into (2), α is calculated as

$$\alpha = \chi\sqrt{\omega_1\omega_2}\frac{\omega_{22} + \omega_{11}}{\omega_2 - \omega_1}\left(\frac{1}{\omega_1\omega_2} - \frac{1}{\omega_{22}\omega_{11}}\right). \tag{8}$$

The filter parameters in Fig. 4 can be obtained with (4), (5), and (8):

$$L_{11} = \frac{g_1}{\alpha\gamma\beta}, \quad C_{11} = \frac{1}{\beta\chi L_{11}}, \tag{9}$$

$$L_{12} = \frac{g_1\gamma}{\alpha\beta}, \quad C_{12} = \frac{1}{\beta\chi L_{12}}, \tag{10}$$

$$L_{21} = \frac{\alpha\gamma}{\chi g_2}, \quad C_{21} = \frac{1}{\beta\chi L_{21}}, \tag{11}$$

$$L_{22} = \frac{\alpha}{g_2\gamma\chi}, \quad C_{22} = \frac{1}{\beta\chi L_{22}}. \tag{12}$$

The parallel-resonator-based filter elements including the J-inverters in Fig. 3(c) are calculated from the filter circuit in Fig. 4 as follows:

When (13) and (14), as shown at the bottom of the next page are equal, the J-inverters have

$$J_{01} = \sqrt{\frac{Y_0 C_{a1}}{g_0 L_{11}}}, \quad J_{23} = \sqrt{\frac{Y_0 C_{a2}}{g_3 C_{21}}}, \tag{15}$$

$$J_{12} = \sqrt{\frac{C_{a1}C_{a2}}{L_{11}C_{21}}}, \quad J_a = \sqrt{\frac{C_{a1}C_{x1}}{L_{11}C_{12}}}, \tag{16}$$

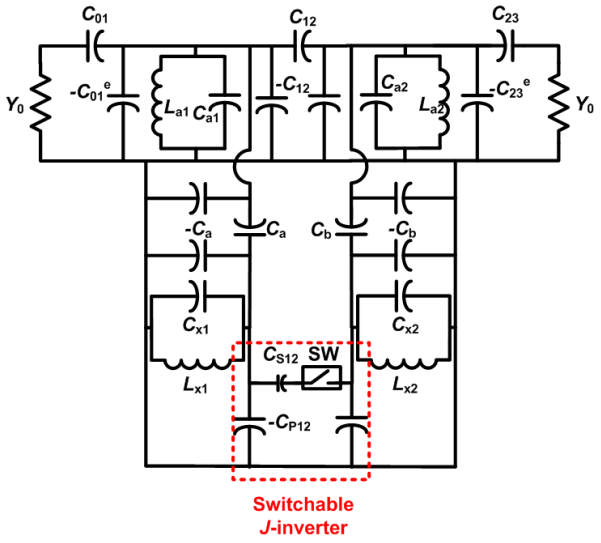

FIGURE 5. Switchable-band bandpass filter circuit using capacitor-type *J*-inverters.

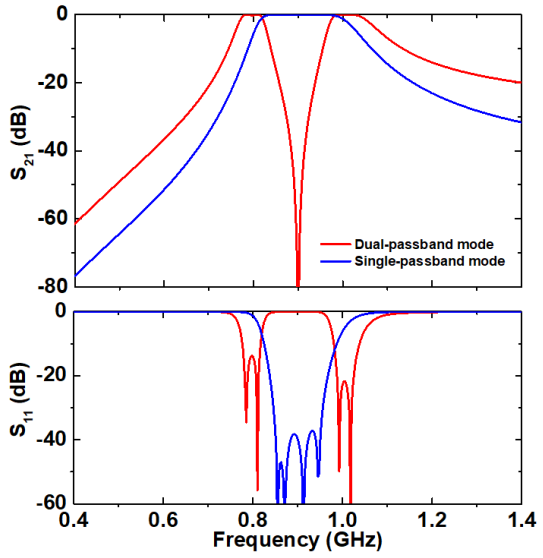

FIGURE 6. Simulated result of the filter circuit in Fig. 5.

$$J_b = \sqrt{\frac{C_{x2}C_{a2}}{C_{21}L_{22}}}. \tag{17}$$

When capacitor-type J-inverters are implemented in the filter in Fig. 2, the filter configuration in Fig. 5 is accomplished [12]. The filter in Fig. 5 is designed based on (15)–(17) with 0.01 dB Chebyshev ripple at $f_1 = 0.8$ GHz and $f_2 = 1.0$ GHz, $f_{11} = 0.798$ GHz and $f_{22} = 1.02$ GHz in Fig. 3(c). The filter parameters for the dual-passband mode are $C_{01} = C_{23} = 1.92$ pF, $C_{01}^{e} = C_{23}^{e} = 1.49$ pF, $C_{12} = 0.84$ pF, $C_a = C_b = 1.79$ pF, $C_{P12} = 0.84$ pF, switch (SW) = off-state, $C_{a1} = C_{x1} = C_{a2} = C_{x2} = 8$ pF, and $L_{a1} = L_{x1} = L_{a2} = L_{x2} = 3.96$ nH. The C_{S12} value is 0 pF, since SW is in the off-state.

The filter elements for the four-pole single-passband mode are extracted with 0.01 dB Chebyshev ripple at a center frequency of 0.9 GHz with a fractional bandwidth of 0.15 as $C_{01} = C_{23} = 3.33$ pF, $C_{01}^{e} = C_{23}^{e} = 1.77$ pF, $C_{12} = 0.1$ pF, $C_a = C_b = 1.28$ pF, $C_{S12} = C_{P12} = 0.94$ pF, SW = on-state, $C_{a1} = C_{x1} = C_{a2} = C_{x2} = 7.9$ pF, and $L_{a1} = L_{x1} = L_{a2} = L_{x2} = 3.96$ nH [12].

The filter with the switchable two-pole dual- / four-pole single-passband responses is accomplished using the single switch-connected J-inverter in series, as shown in Fig. 6.

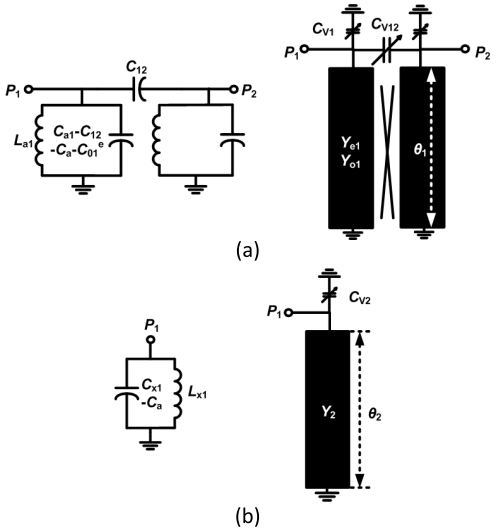

FIGURE 7. Transmission-line resonator transformations of (a) the lumped-coupled resonator pairs and (b) the lumped parallel resonator.

In the dual-passband mode, the high isolation between the two passbands is obtained as 80 dB at 0.9 GHz.

C. TUNABLE FILTER DESIGN

The lumped resonators in Fig. 5 are transformed into the distributed resonators in Fig. 7(a) and (b) to realize a microstrip

$$\frac{Y_{in1}}{g_0} = \frac{1/g_0}{j\left(\omega L_{11} - \frac{\beta\chi L_{11}}{\omega}\right) + \frac{1}{j\left(\omega C_{12} - \frac{\beta\chi C_{12}}{\omega}\right)} + \frac{1}{j\left(\omega C_{21} - \frac{\beta\chi C_{21}}{\omega}\right) + \frac{1}{j\left(\omega L_{22} - \frac{\beta\chi L_{22}}{\omega}\right)} + \frac{1}{g_3}}}, \tag{13}$$

$$\frac{Y_{in2}}{Y_0} = \frac{J_{01}^2/Y_0}{j\left(\omega - \frac{\beta\chi}{\omega}\right)C_{a1} + \frac{J_a^2}{j\left(\omega - \frac{\beta\chi}{\omega}\right)C_{x1}} + \frac{J_{12}^2}{j\left(\omega - \frac{\beta\chi}{\omega}\right)C_{a2} + \frac{J_b^2}{j\left(\omega - \frac{\beta\chi}{\omega}\right)C_{x2}} + \frac{J_{23}^2}{Y_0}}}. \tag{14}$$

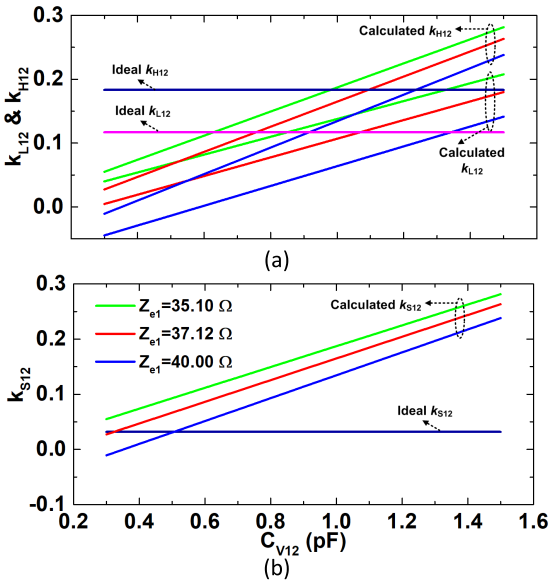

FIGURE 8. Coupling coefficients calculated for the circuits in Fig. 7 for (a) the dual-passband mode and (b) the single-passband mode. (Z_{o1} = 35Ω, C_{V1} = 2.8 pF, θ_1 = 50°).

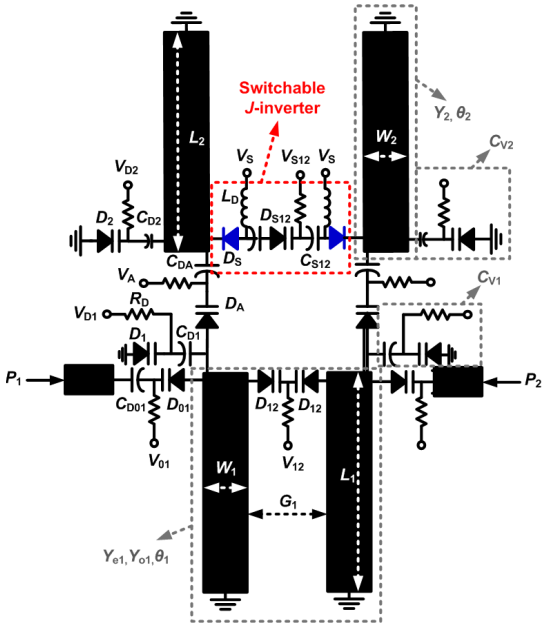

FIGURE 9. Proposed filter configuration.

tunable filter. The capacitor-coupled lumped resonator pairs can be changed to a combline coupled line with a coupling capacitor (C_{V12}) (see Fig. 7(a)). The parallel lumped resonator is replaced with a capacitor-loaded short-circuited transmission line (see Fig. 7(b)).

(18) and (19) are extracted from the input impedances and slope parameters of the circuits in Fig. 7(a), respectively [12].

$$\omega C_{V1} - Y_{e1}\cot\theta_1 = \omega C_{ra1} - \frac{1}{\omega L_{a1}}, \tag{18}$$

$$\frac{\omega_0}{2}C_{V1} + Y_{e1}\frac{A\omega_0}{2}\csc^2\theta_1 = \frac{1}{\omega_0 L_{a1}}, \tag{19}$$

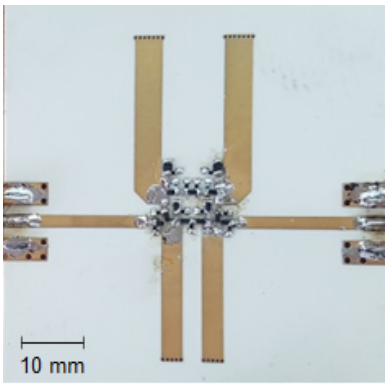

FIGURE 10. Photograph of the fabricated filter.

where $A = \theta_1/\omega_0$ and $C_{ra1} = C_{a1}$ - C_{12} - C_a - C^e_{01}. Therefore, Y_{e1} and C_{V1} are calculated from (18) and (19) as follows:

$$Y_{e1} = \frac{\frac{3}{\omega_0^2 L_{a1}} - C_{ra1}}{A\csc^2\theta_1 + \frac{\cot\theta_1}{\omega_0}}, \tag{20}$$

$$C_{V1} = \frac{2}{\omega_0^2 L_{a1}} - AY_{e1}\csc^2\theta_1. \tag{21}$$

C_{V12} is also derived as reported in [12].

$$C_{V12} = C_{12} + \frac{Y_{o1} - Y_{e1}}{2\omega_0}\cot\theta_1. \tag{22}$$

Y_2 and C_{V2} in Fig. 7(b) are calculated similarly to in (20) and (21).

$$Y_2 = \frac{\frac{3}{\omega_0^2 L_{x1}} - C_{rx1}}{B\csc^2\theta_2 + \frac{\cot\theta_2}{\omega_0}}, \tag{23}$$

$$C_{V2} = \frac{2}{\omega_0^2 L_{x1}} - B\csc^2\theta_2, \tag{24}$$

where $B = \theta_2/\omega_0$ and $C_{rx1} = C_{x1}$ - C_a.

The coupling coefficients of the circuits in Fig. 7(a) are calculated based on (19) and (22) as shown in Fig. 8(a) and (b) [12]. k_{L12} and k_{H12} are the low- and high-band coupling coefficients respectively, for the dual-passband mode; k_{s12} is for the single-passband mode. C_{12}, C_a, C^e_{01}, L_{a1}, and C_{a1} in Fig. 7(a) are used as the values extracted in II.B. When C_{V12} = 1.05 pFs and Z_{e1} = 37.12 Ω in Fig. 8(a), the k_{L12} and k_{H12} values for the transmission-line circuit are equal to the values for the lumped circuits. In addition, when C_{V12} = 0.33 pF and Z_{e1} = 37.12 Ω in Fig. 8(b), k_{S12} of the transmission-line circuit is the same as that of one of the lumped circuits. Therefore, the lumped circuits in Fig. 5 are replaced with the proposed distributed structures.

As shown in Fig. 9, the proposed tunable filter configuration is accomplished by implementing the distributed resonators in Fig. 7 in the circuit in Fig. 5. The coupled resonator pairs consisting of C_{ra1} (= C_{a1} - C_{12} - C_a - C^e_{01})/L_{a1}, C_{ra2}/L_{a2}, and C_{12} are transformed into a varactor-loaded coupled line (Y_{e1}, Y_{o1}, θ_1, and D_1 + C_{D1}) with a coupling varactor (D_{12}) based on (20)–(22). The parallel lumped

TABLE 1. Performance Comparison With Other Filters.

	Switchable-band design method	Tuning range (GHz)	Minimum frequency separation ratio	Insertion loss (dB)	Number of poles (single- /dual-passband mode)	Attenuation level @ a frequency removing one of the two passbands (dB)
[6]	Impedance mismatching method (electrical control)	0.76-1.78/ 1.6-2.63	3.57 (0.7:2.5)	2.2-4.78	2/2	13
[7]	Membrane shorting method (Mechanical control)	2-3/ 8-9	2.67 (3:8)	0.9-1.5	2/2	35
[8]	Control of frequencies for poles (electrical control)	1.0-1.29/ 1.4-1.58	1.24 (1.25/1.55)	2.1-5.5	4/2	25
This Work	Single switchable J-inverter (electrical control)	0.69-0.9/ 0.85-1.07	1.11 (0.9:1)	2.9-4.9	4/2	42

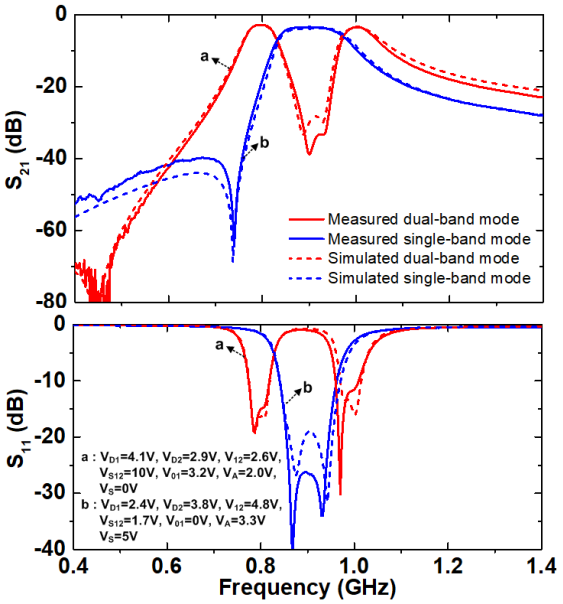

FIGURE 11. Simulated and measured results of the filter in Fig. 10.

resonator ($C_{rx1} = C_{x1}$ - C_a and L_{x1}) is realized with the varactor-loaded short-circuited resonator (Y_2, D_2 + C_{D2}, and θ_2) based on (23) and (24). The switchable J-inverter consists of two PIN diodes (D_S), one varactor (D_{S12}), and two DC-blocking capacitors (C_{S12}). Two PIN diodes are used to obtain sufficient isolation between the two varactor-loaded short-circuited resonators, and C_{P12} in the switchable J-inverter is absorbed into the short-circuited resonator (Y_2 and θ_2). C_{D01} and D_{01} are used as the input/output J-inverter (C_{01} and C_{23}). C_a and C_b are also implemented as a varactor (D_A) and a DC-blocking capacitor (C_{DA}).

The tunable bandpass filter with the switchable four-pole single- / two-pole dual-passband modes is designed with 0.01 dB Chebyshev ripple at $f_1 = 0.8$ GHz and $f_2 = 1.0$ GHz, and with $f_{11} = 0.798$ GHz and $f_{22} = 1.02$ GHz, as mentioned in section II.B (single passband mode: center frequency of 0.9 GHz with a fractional bandwidth of 0.15). The design parameters are calculated based on (20)–(24) as follows: $Z_{e1} = 1/Y_{e1} = 37.12\ \Omega$, $Z_{o1} = 1/Y_{o1} = 35\ \Omega$, $C_{V1} = 2.8$ pF, $C_{V12} = 1.05$ pF, $\theta_1 = 50°$ at 1.28 GHz ($= 1/2\pi\sqrt{C_{ra1}L_{a1}}$), $Z_2 = 1/Y_2 = 29.3\ \Omega$, $C_{V2} = 4.48$ pF, and $\theta_2 = 50°$ at 1.015 GHz ($= 1/2\pi\sqrt{C_{rx1}L_{x1}}$). The filter is fabricated on a 30 mil Duroid substrate ($\varepsilon_r = 3.48$, Rogers RT/Duroid 4350). The filter dimensions are obtained based on the transmission-line parameters as follows: $G_1 = 1.48$ mm, $L_1 = 8.0$ mm, $L_2 = 9.7$ mm, $W_1 = 1.9$ mm, and $W_2 = 1.4$ mm.

An SMV1234 varactor ($C = 9.63$–1.32 pF, $R_S = 0.8\ \Omega$) is used as D_1, D_3, and D_{01} to obtain the required capacitance. An SMV1232 ($C = 4.15$–0.75 pF, $R_S = 1.5\ \Omega$) is selected as D_{12} and D_{S12}. The PIN diode (D_S) for the switchable J-inverter is an SMP1345-040 ($C_T = 0.18$ pF at 5 V, $R_S = 1.5\ \Omega$ at 10 mA). DC biasing is implemented using a 10 kΩ resistor (R_D) to reduce the RF-signal leakage through the bias network. ATC600L chip capacitors ($R_S = 0.12\ \Omega$, $C_{D1} = 10$ pF, $C_{D2} = 15$ pF, $C_{DA} = 15$ pF, $C_{D01} = 5.6$ pF, $C_{S12} = 3$ pF, and $Q = 100$ at 1 GHz) are used. Toko FH18NJ inductor ($R_S = 0.5\ \Omega$, $L = 18$ nH, SRF = 2.35 GHz) is used for L_D. Full-wave results are obtained by simulating the filter with the simplified model of the varactors in the Agilent Advanced Design System (ADS).

III. MEASURED RESULTS

Fig. 10 shows a photograph of the fabricated filter. Fig. 11 presents the simulated and measured filter S-parameters. The two-pole dual-band and four-pole single-band responses are shown in the proposed filter. The measured results agree well with the simulated results. When the switch (D_S) is in the off-state, the center frequencies of the dual-passband mode are 0.8 GHz and 1.0 GHz. The insertion losses at 0.8 GHz and 1.0 GHz are 3.0 dB and 3.1 dB, respectively, and are mostly due to the varactor Q. The rejection level between the two passbands is 37 dB at 0.9 GHz. In contrast, when the switch (D_S) is in the on-state, the single-passband response is shown at the center frequency of 0.9 GHz, and the insertion loss is 3.4 dB. In the single-passband mode, a transmission zero is created at

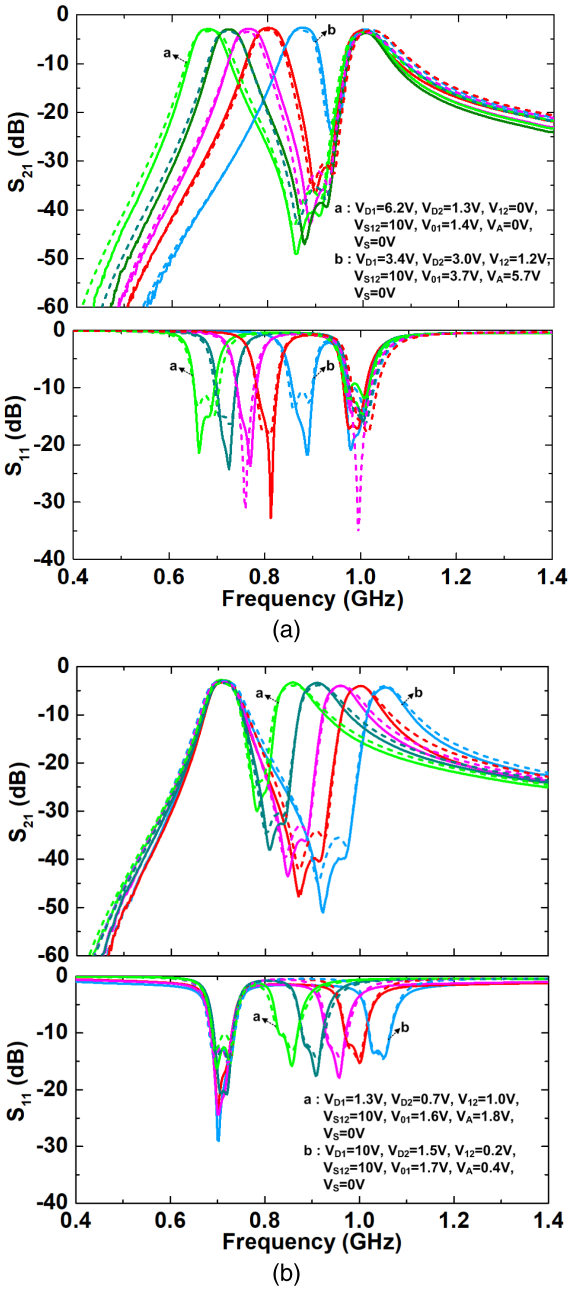

FIGURE 12. Dual-passband mode measured and simulated results for (a) the low-passband tuning and (b) the high-passband tuning. (Solid line: measurements, and dotted line: simulations).

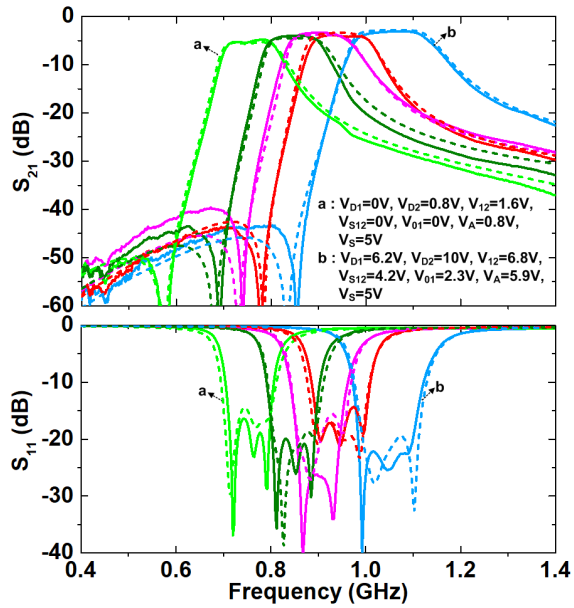

FIGURE 13. Single-passband mode measured and simulated results (Solid line: measurements, and dotted line: simulations).

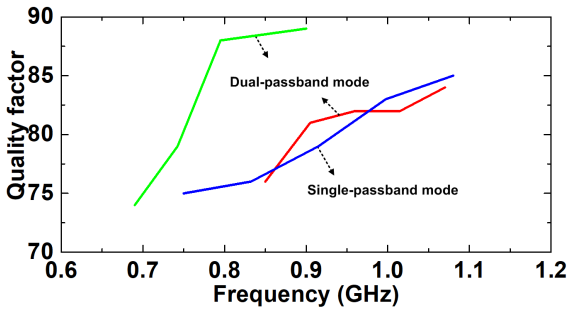

FIGURE 14. Quality factors calculated for the proposed filter in Fig. 10.

0.75 GHz due to the parallel resonance by the varactor (D_{12}) and the magnetic coupling of the coupled line (Y_{e1} and Y_{o1}). The attenuation level is 68 dB at 0.75 GHz.

The measured center frequency tuning of the dual-passband mode is shown in Fig. 12(a) and (b). The two center frequencies can be independently controlled. The low passband center frequency is tuned from 0.69 to 0.9 GHz with a 1 dB bandwidth of 75–88 MHz and an insertion loss of 2.9–3.1 dB (see Fig. 12(a)). The high-passband center frequency covers 0.85–1.07 GHz with a 1 dB bandwidth of 80–92 MHz (see Fig. 12(b)). The high-passband insertion loss is 3.0–3.9 dB. The transmission zeros are located between the two passbands due to the series resonance of the varactor (D_A) and the short-circuited resonator (Y_2 and θ_2). Therefore, the attenuation levels higher than 20 dB are yielded between the two passbands.

Fig. 13 shows the center frequency tuning for the single-passband mode. The center frequency is tuned from 0.75 to 1.08 GHz. The 1 dB bandwidth is 105–158 MHz, and an insertion loss of 3.5–4.9 dB is obtained due to the series resistance in the PIN diode as well as the varactor Q. The transmission zero is located on the band lower than the center frequency, and the attenuation level higher than 60 dB can be obtained.

The resonator Q is calculated based on the measured insertion losses in Figs. 12 and 13 and is shown in Fig. 14 [12]. In the dual-passband mode, the resonator Q is 74–89, whereas in the single-passband mode, it is 75–85. The filter insertion loss is limited by the varactor Q.

Table 1 shows the comparison between the proposed filter and the conventional tunable band-switchable filters [6]–[8].

In the proposed filter, the tuned switchable-band response is easily obtained using the single switchable J-inverter. When two center frequencies for the dual-passband mode are in proximity (minimum frequency separation ratio = 1.11), the high attenuation level is maintained. Moreover, when one of the two passbands is removed in order to achieve the single-passband mode, the high stopband attenuation level is shown to be 42 dB.

IV. CONCLUSION

In this article, a switchable dual-/single-band tunable bandpass filter is demonstrated. The single-to-dual passband is effectively transformed based on a single switchable J-inverter consisting of two PIN diodes and a varactor. Two-pole dual passbands are accomplished based on the filter prototype using series and parallel lumped resonators, and the four-pole single passband is obtained by adjusting the J-inverter values. The center frequency tuning and passband transformation are controlled by the varactors and PIN diode.

In the future, RF MEMS switched capacitors can be used to result in the significant improvement in insertion loss.

REFERENCES

[1] B. Wang and K. J. Ray Liu, "Advances in cognitive radio networks: A survey," *IEEE J. Sel. Topics Signal Process.*, vol. 5, no. 1, pp. 5–23, Feb. 2011.
[2] P.-H. Deng and J.-H. Jheng, "A switched reconfigurable high-isolation dual-band bandpass filter," *IEEE Microw. Wireless Compon. Lett.*, vol. 21, no. 2, pp. 71–73, Feb. 2011.
[3] J. Xu, "A microstrip switchable filter with four operating modes," *IEEE Microw. Wireless Compon. Lett.*, vol. 26, no. 2, pp. 101–103, Feb. 2016.
[4] T. Yang and G. M. Rebeiz, "Three-pole 1.3–2.4-GHz diplexer and 1.1–2.45-GHz dual-band filter with common resonator topology and flexible tuning capabilities," *IEEE Trans. Microw. Theory Techn.*, vol. 61, no. 10, pp. 3613–3624, Oct. 2013.
[5] R. Gomez-Garcia, A. C. Guyette, D. Psychogiou, E. J. Naglich, and D. Peroulis, "Quasi-elliptic multi-band filters with center-frequency and bandwidth tunability," *IEEE Microw. Wireless Compon. Lett.*, vol. 26, no. 3, pp. 192–194, Mar. 2016.
[6] D. Lu, X. Tang, N. S. Barker, and Y. Feng, "Single-band and switchable dual-/single-band tunable BPFs with predefined tuning range, bandwidth, and selectivity," *IEEE Trans. Microw. Theory Techn.*, vol. 66, no. 3, pp. 1215–1227, Mar. 2018.
[7] B. Lee, B. Koh, S. Nam, T.-H. Lee, and J. Lee, "Band-switchable substrate-integrated waveguide resonator and filter," *IEEE Trans. Microw. Theory Techn.*, vol. 66, no. 1, pp. 147–156, Jan. 2018.
[8] Y. Cho, S. Yun, and C. Park, "A 1.0 to 1.58-GHz tunable bandpass filter with switchable single-/dual-band responses," *Microw. Opt. Technol. Lett.*, vol. 62, no. 11, pp. 3438–3443, Nov. 2020.
[9] Y.-H. Cho, X.-G. Wang, and S.-W. Yun, "Design of dual-band interdigital bandpass filters using both series and shunt resonators," *IEEE Microw. Wireless Compon. Lett.*, vol. 22, no. 3, pp. 111–113, Mar. 2012.
[10] X. Guan, Z. Ma, P. Cai, Y. Kobayashi, T. Anada, and G. Hagiwara, "Synthesis of dual-band bandpass filters using successive frequency transformations and circuit conversions," *IEEE Microw. Wireless Compon. Lett.*, vol. 16, no. 3, pp. 110–112, Mar. 2006.
[11] H. Uchida, H. Kamino, K. Totani, N. Yoneda, M. Miyazaki, Y. Konishi, S. Makino, J. Hirokawa, and M. Ando, "Dual-band-rejection filter for distortion reduction in RF transmitters," *IEEE Trans. Microw. Theory Techn.*, vol. 52, no. 11, pp. 2550–2556, Nov. 2004.
[12] G. L. Matthaei, E. Young, and E. M. T. Jones, *Microwave Filters, Impedance-Matching Networks, and Coupling Structures*. Norwood, MA, USA: Artech House, 1980.
[13] M. A. El-Tanani and G. M. Rebeiz, "High-performance 1.5–2.5-GHz RF-MEMS tunable filters for wireless applications," *IEEE Trans. Microw. Theory Techn.*, vol. 58, no. 6, pp. 1629–1637, Jun. 2010.

YOUNG-HO CHO (Member, IEEE) received the B.Eng. and Ph.D. degrees in electronic engineering from Sogang University, Seoul, South Korea, in 2005 and 2012, respectively. From 2013 to 2014, he was a Postdoctoral Researcher with the Department of Electrical and Computer Engineering, University of California at San Diego (UCSD), La Jolla, CA, USA. From 2015 to 2018, he was a Senior Researcher with the Defense Industry Technology Center (DITC), Agency for Defense Development (ADD), Seoul, South Korea. He is currently an Assistant Professor with the Electrical and Communication Engineering Department, Daelim University, Anyang, South Korea. His research interests include RF filters, tunable and multi-band circuits, antennas, and RF systems.

CHEOLSOO PARK (Member, IEEE) received the B.Eng. degree in electrical engineering from Sogang University, Seoul, South Korea, the M.Sc. degree from the Biomedical Engineering Department, Seoul National University, Seoul, and the Ph.D. degree in adaptive nonlinear signal processing from Imperial College London, London, U.K., in 2012. From 2012 to 2013, he was a Postdoctoral Researcher with the University of California at San Diego, San Diego. He is currently an Associate Professor with the Computer Engineering Department, Kwangwoon University, Seoul. His research interests include machine learning and adaptive and statistical signal processing, with applications in healthcare, computational neuroscience, and wearable technology.

SANG-WON YUN (Life Member, IEEE) received the B.Sc. and M.Sc. degrees in electronic engineering from Seoul National University, Seoul, South Korea, in 1977 and 1979, respectively, and the Ph.D. degree in electrical engineering from The University of Texas at Austin, Austin, in 1984. Since 1984, he has been a Professor with the Department of Electronic Engineering, Sogang University, Seoul. From January 1988 to December 1988, he was a Visiting Professor with The University of Texas at Austin. From 2009 to 2011, he was with the Korea Communications Commission (KCC) as a Project Manager. From 2000 to 2004, He was the Chairman of the IEEE Microwave Theory and Techniques Society (IEEE MTT-S) Korea Chapter. In 2008, he was the President of the Korea Institute of Electromagnetic Engineering and Science (KIEES). His research interests include microwave and millimeter-wave devices and circuits.